Phys Chem Minerals (2005) 32: 442–449
DOI 10.1007/s00269-005-0020-7

ORIGINAL PAPER

Ruslan P. Liferovich · Roger H. Mitchell

Rhombohedral ilmenite group nickel titanates with Zn, Mg, and Mn: synthesis and crystal structures

Received: 24 February 2005 / Accepted: 29 June 2005 / Published online: 30 August 2005

Abstract Binary, ternary, and quaternary rhombohedral ordered titanates, $Ni_{1/2}Mn_{1/2}TiO_3$, $Ni_{1/2}Mg_{1/2}TiO_3$, $Ni_{1/3}Zn_{1/3}Mg_{1/3}TiO_3$, and $Ni_{1/4}Zn_{1/4}Mg_{1/4}Mn_{1/4}TiO_3$, were obtained by solid-state synthesis at 1095°C at ambient pressure in a nitrogen atmosphere. All of the compounds adopt $ATiO_3$ (A = Ni, Mn, Zn, and Mg) stoichiometry. Crystal structures were refined by the Rietveld method from powder X-ray diffraction data. Unit cell parameters and unit cell volumes decrease with decreasing average radius of the $^{vi}A^{2+}$ cation. All the synthetic titanates adopt the space group $R\bar{3}$ and the ilmenite structure consisting of distorted AO_6 and TiO_6 octahedra. The divalent cations and Ti^{4+} are distributed in layers of octahedra alternating along c with no evidence for disorder. In common with pyrophanite, $NiTiO_3$, and ilmenite sensu stricto, the distortion of the AO_6 octahedra is less than that of the TiO_6 octahedra. The Ti^{4+} and A-site cations in the titanates are off-centred within the coordination polyhedra. Deviation of the z positional parameters from their theoretical values for the A and Ti atoms indicate that in the titanates with the larger A^{2+} cations and Goldschmidt tolerance factors, $t \geq 0.745$, the AO_6 octahedral layer is more "puckered" above and below planes parallel to (001) than that of the TiO_6 octahedra, and vice versa in the titanates with smaller R_A^{2+} for which $t \leq 0.745$. Data are given for the volumes and distortion indices of all the coordination polyhedra. This study confirms the existence and stability of complex solid solutions between ordered rhombohedral titanates of Ni and first-row transition metals at ambient conditions over a range of t from 0.786 to 0.737. These experimental data suggest that the formation of ilmenite-type titanates enriched in Ni is possible in exotic mineral-forming systems at low pressure and/or in extraterrestrial rocks.

Keywords Titanates · Nickel · X-ray diffraction · Crystal structures · Ordering · Ilmenite

R. P. Liferovich · R. H. Mitchell (✉)
Department of Geology, Lakehead University,
955 Oliver Road, Thunder Bay, ON, P7B 5E1,
Canada
E-mail: rmitchel@lakeheadu.ca
Tel.: +1-807-3438287
Fax: +1-807-3467853

Introduction

Nickel titanate, $NiTiO_3$, is known to adopt the ilmenite structure and is stable at ambient conditions (Ohgaki et al. 1988; and references therein). The results of our research on the crystal chemistry of complex ternary oxides, ABO_3, demonstrates the existence and stability of quenched quinary titanates of Co, Mg, Mn, Ni, and Zn, which are isostructural with ilmenite (*in preparation*). These preliminary data indicate that $NiTiO_3$ could form continuous solid solutions with other $A^{2+}TiO_3$ titanates of Mg, Mn, and Zn (geikielite, pyrophanite, and ecandrewsite end members of the ilmenite group of minerals, respectively).

Ni has been reported as a significant constituent of natural ilmenite-group minerals only in exotic ignimbrites from the Saaksjarvi impact structure, southwestern Finland (Badjukov et al. 2001). To date, structural and/or compositional data on ilmenite-structured natural and synthetic nickeliferous titanates of the first-row transition metals have not been reported.

This study has four objectives: (1) to demonstrate the existence and stability of the completely ordered rhombohedral titanates of Ni in combination with other transition metals; (2) to describe a synthesis procedure which will be useful for further studies; (3) to characterize the crystal structure of complex Ni-titanates and outline their crystal structure evolution resulting from the combination of Ni with other transition metals; (4) to demonstrate the absence of compositionally driven phase transitions in the $ATiO_3$ compounds involving Ni, and absence of disorder between $^{vi}A^{2+}$ and $^{vi}Ti^{4+}$ cations in their structures.

The ilmenite structure

The ilmenite structure is an ordered derivative of the *archetype* corundum structure. Typically, the ilmenite-type structure is adopted by $A^{2+}Ti^{4+}O_3$ compounds when $^{vi}R_A$ is much smaller than radius of the oxygen anion resulting in a Goldshmidt tolerance factor, t (Goldschmidt 1926), close to 0.75 (Mitchell 2002). The structure is based on *hcp* oxygen layers with cations occupying two-thirds of the available octahedral interstices. In contrast to the fully disordered corundum structure (space group $R\bar{3}c$), the ilmenite structure contains equal amounts of di- and tetravalent cations, ordered along the octahedron layers and alternating along the c-dimension of the unit cell. In terms of lateral nearest-neighbour A–A and Ti–Ti cation–cation distances within the (001) layers, the cations are arranged in regular hexagonal rings (Harrison et al. 2000). A pair of AO_6 and TiO_6 octahedra shares a (001) face (Fig. 1a), and each octahedron in the ilmenite structure shares an edge with the same-type of octahedra, and three edges with the other type octahedra. The stacking sequence along $[001]_h$ of this structure is ″*A*-Ti-□-Ti-*A*-□″ (where ″□″ stands for a vacant site), and ″Ti-Ti-□″ or ″*A*-*A*-□″ parallel to (111), resulting in a $R\bar{3}$ rhombohedral cell. Due to repulsive Ti–Ti and A–Ti interactions across the shared faces and edges of octahedra (Wechsler and Prewitt 1984; Ko and Prewitt 1988; Harrison et al. 2000, etc.), the (001) layers of octahedra are "puckered" so that adjacent cations are displaced up and down the [001] axis (Fig. 1b).

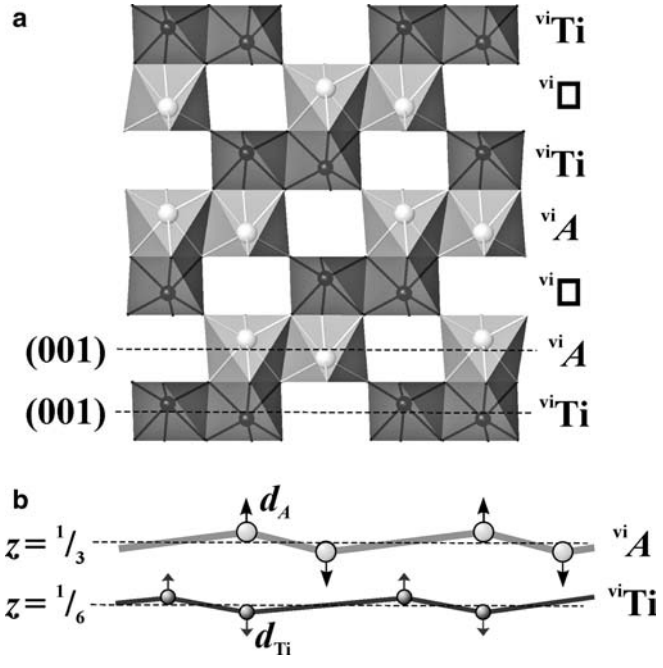

Fig. 1 Projection onto the $(1\bar{1}0)$ plane of portions of the structure of $R\bar{3}$-structured synthetic $Ni_{1/2}Mg_{1/2}TiO_3$ (A = $Ni_{1/2}Mg_{1/2}$, this study), illustrating **a** the ordering and disposition of the face and corner-sharing octahedra, **b** the "puckering" of the layers of octahedra above and below parallel to (001)

In common with corundum, displacement of the cations in the $R\bar{3}$ structure from the centroids of both types of octahedra results in distortion of the coordination polyhedra. Various styles of distortion are known for ilmenite-structured compounds (Mitchell 2002). The AO_6 polyhedron can be more distorted than the TiO_6 polyhedron or vice versa, e.g. in ilmenite (sensu stricto) distortion of the FeO_6 octahedron is significantly less than that of the TiO_6 octahedron (Mitchell 2002). Further distortion of the corundum structure in the case of $A^{2+}Ti^{4+}O_3$ compounds can be driven by an increase in pressure. This distortion results in a phase transition to a structure with the ″*A*-Ti-□-A-Ti-□″ stacking sequence, both along and orthogonal to $[001]_h$, with the A^{2+} and Ti^{4+} cations occupying $[001]_h$-alternating layers. Such a structure has a $R3c$ rhombohedral cell and is similar to that of $LiNbO_3$. This structure differs in the mode of connection of octahedra from that of the ilmenite structure (Mitchell 2002).

Examples of the $R\bar{3} \rightarrow R3c$ phase transition are the high-pressure transformations of pyrophanite, geikielite, ilmenite, and $NiTiO_3$ (Syono et al. 1969; Ko and Prewitt 1988; Boysen et al. 1995; Linton et al. 1999). With further compression, $ATiO_3$ compounds may undergo a further phase transition to *Pbnm*-structured perovskite isostructural with $GdFeO_3$ (Linton et al. 1999). Phase transformations between the ilmenite, lithium niobate and perovskite structures are complex and their study is hindered by kinetic factors and hysteresis effects (Mitchell 2002). $NiTiO_3$ is the only ternary titanate for which a temperature-driven second order phase transition has been described and studied in detail. The $R\bar{3} \rightarrow R\bar{3}c$ transformation takes place at $T \geq 1287$°C (Lerch et al. 1991, 1992; Lerch and Laqua 1992; Boysen et al. 1995).

The present study was undertaken to confirm the existence and stability of the completely ordered binary, ternary, and quaternary titanates of Ni and first-row transition metals other than Fe, and to study the response of ilmenite-type structure to entry of cations ranging in radii from 0.83 to 0.69Å [Mn^{2+} and Ni^{2+}, respectively (Shannon 1976)] at the $^{vi}A^{2+}$ site resulting in variation of the Goldschmidt tolerance factor from 0.786 to 0.737 (Table 1). Detailed discussion of possible complex interactions such as first order and second order Jahn–Teller effects, "direct $^{vi}A^{2+}$–$^{vi}A^{2+}$ and/or $^{vi}Ti^{4+}$–$^{vi}Ti^{4+}$ interactions", mechanisms of the repulsive Ti–Ti and A–Ti interactions across the shared faces and edges of octahedra and/or "metal–metal bonding ($^{vi}A^{2+}$–$^{vi}Ti^{4+}$) along the threefold axes" in the transition metal titanates (Goodenough 1960; Wechsler and Prewitt 1984; Ko and Prewitt 1988; Ohgaki et al. 1988; Kunz and Brown 1995; Harrison et al. 2000; Mitchell 2002) are beyond the scope of this study.

Table 1 Selected refinement parameters and crystallographic characteristics of synthetic titanates at ambient conditions

		1	*2*	*3*	*4*	*5*	*6*
$^{vi}R_A^{2+}$	Å	0.830	0.760	0.745	0.717	0.705	0.690
t^a		0.786	0.762	0.756	0.747	0.742	0.737
Phase composition							
AtiO$_3$	%	99.2(1)	99.33(1)	98.4(1)	92.8(1)	93.8(2) *Ru* 3.3(2)	95.7(1)
Other phases	%	0.8(1)	*Ru* 0.7(1)	*Ru* 1.6(1)	*Ru* 1.9(1) *Sp* 5.3(1)	*Arm* 1.6(1) *AO* 1.3(1)	*Ru* 2.8(1) *A*O 1.5(1)
Agreement factors							
n		30	30	30	36	42	36
R_{exp}	%	11.93	8.72	8.35	7.05	7.24	6.68
R_p	%	11.01	8.99	8.54	8.60	8.39	8.29
R_{Bragg}	%	2.63	2.93	2.45	2.58	2.47	2.22
R_{wp}	%	14.52	11.44	11.01	10.79	8.39	9.98
χ^2		1.21	1.31	1.32	1.53	1.47	1.48
DW		1.49	1.31	1.28	1.02	1.10	1.02
Unit cell parameters in space group $R\bar{3}$							
a	Å	5.1386(0)	5.0855(0)	5.0770(0)	5.0544(0)	5.0418(0)	5.0321(1)
c	Å	14.2857(2)	14.0191(1)	13.9727(1)	13.8737(1)	13.8494(1)	13.7924(2)
c/a		2.780	2.757	2.752	2.745	2.747	2.741
V	Å^3	326.682(6)	313.996(4)	311.910(5)	306.953(5)	304.885(4)	302.456(12)
Coordination polyhedra characteristics							
$< A$–O1 $>$	Å	2.196(11)	2.141(13)	2.129(14)	2.121(13)	2.095(8)	2.088(10)
V_{AO6}	Å^3	13.379(7)	12.583(7)	12.312(8)	12.273(7)	11.933(5)	11.826(6)
d_A	Å	0.38	0.31	0.34	0.31	0.26	0.24
Δ_{AO6}		1.91	0.68	1.52	1.28	0.43	0.193
δ_{AO6}		126.6	94.0	102.2	85.6	65.7	62.3
$<$Ti–O1$>$	Å	1.981(11)	1.973(13)	1.983(14)	1.966(12)	1.976(8)	1.968(11)
V_{TiO6}	Å^3	10.006(7)	9.824(6)	10.036(7)	9.750(6)	9.908(4)	9.763(5)
d_{Ti}	Å	0.27	0.30	0.29	0.30	0.30	0.31
Δ_{TiO6}		2.81	3.16	3.66	3.48	3.69	3.15
δ_{TiO6}		84.4	95.9	83.9	90.6	88.6	95.1

1 $MnTiO_3$; *2* $Ni_{1/2}Mn_{1/2}TiO_3$; *3* $Ni_{1/4}Mn_{1/4}Zn_{1/4}Mg_{1/4}TiO_3$; *4* $Ni_{1/3}Zn_{1/3}Mg_{1/3}TiO_3$; *5* $Ni_{1/2}Mg_{1/2}TiO_3$; *6* $NiTiO_3$

Ru Rutile, *Sp* spinel, *A*O bunsenite-like solid solution (A = Ni, Mg), *Arm* armalcolite

$^{vi}R_A^{2+}$ average radius of cations in A site

n Number of independent parameters

d_i the distance to the central atom

Δ_n polyhedron bond length distortion (see text for details)

δ_n bond angle variance (see text for details)

$R_{exp} = [(N-P)/(\Sigma w_i y_{i(obs)}2)]^{1/2}$

$R_p = [\Sigma w_i | y_{i(obs)} - y_{i(calc)}|]/\Sigma y_{i(obs)}$

$R_{Bragg} = (\Sigma | I^{1/2}_{k(obs)} - I^{1/2}_{k(calc)} |)/(\Sigma I^{1/2}_{k(obs)})$

$R_{wp} = \{[\Sigma w_i (y_{i(obs)} - y_{i(calc)})^2]/[\Sigma w_i (y_{i(obs)})^2]\}^{1/2}$

$\chi^2 = GOF = [\Sigma w_i (y_{i(obs)} - y_{i(calc)})^2]/(N-P)$

DW (Durbin–Watson statistics) $= [\Sigma^N_{i=2}(\Delta y_i - \Delta y_{i-1})^2]/\Sigma^N_{i=1}\Delta y_i^2$

[a]Tolerance factor for ABO_3 compounds, $t = (R_O + R_A)/[\sqrt{2}(R_O + R_B)]$ (Goldschmidt 1926)

Synthesis and analytical methods

The titanates were synthesized from stoichiometric amounts of NiO, $MnCO_3$, ZnO, MgO, and TiO_2 (high-purity grade) by a solid-state ceramic method. The reagents, dried at 120°C (with exception of $MnCO_3$ which was kept at 85°C) for several days, were mixed, ground in an agate mortar under acetone and pelletized at a pressure of 15 tons per cm^2. The mixtures were than calcined for 2 h at 1000°C in a stream of nitrogen. After regrinding, the samples were re-pelletized and then sintered for 12 h at 1095°C in nitrogen and quenched in liquid nitrogen. At every step, two separate pellets of every compound were prepared, and the duplicates were used as ''sacrificing beds'' to isolate the samples from contact with the quartz tube used for the experiment. The homogeneity and composition of all compounds obtained were assessed by back-scattered electron imaging (BSE) and quantitative X-ray energy-dispersive analysis (QEDS) employing a Jeol JSM-5900 scanning electron microscope equipped with a LINK ISIS 300 analytical system incorporating a Super ATW light element detector (133 eV FwHm Mn K). Spectra were processed with LINK ISIS SEMQUANT quantitative software package with full ZAF corrections applied to the raw X-ray data.

Step-scanned X-ray diffraction (XRD) powder patterns of the synthetic products were obtained at room temperature using a Philips 3710 diffractometer with a graphite monochromator (Bragg–Brentano geometry; LP factor 26.37°; 2-mm thick samples were used to avoid background effects from aluminium–glass holders; radiation Cu K_α; 40 kV; 30 mA; 2θ range 10–120°; $\Delta 2\theta$ step 0.02°; time per step 4 s) and APD powder diffraction software. The diffractometer was calibrated with *Si SRM640b* standard as a reference material.

We attempted also to prepare these compounds in air. However, the X-ray profiles obtained for the samples prepared in an open air atmosphere gave poor Ri-

etveld refinements with asymmetrical residual peaks, presumably due to partial oxidation.

X-ray diffraction patterns were inspected using the Bruker AXS software package EVA equipped with the powder diffraction file (Bruker 2001) to identify the phases present and confirm that $R\bar{3}$-structured compounds were obtained. Data were further analysed by the Rietveld method (Rietveld 1969) using the Bruker AXS software package TOPAS 2.1 operated in the fundamental parameters mode (Cheary and Coelho 1992; Coelho 2000; Bruker 2003). This Windows-based software provides significant improvements in the ease of undertaking Rietveld refinements over commonly used DOS-based software such as FULLPROF (Rodriguez-Carvajal 1990) and permits the refinement of several phases simultaneously, an advantage given the presence of minor amounts of impurity compounds in the synthesized materials. Results of Rietveld refinement of laboratory powder X-ray diffraction data using TOPAS 2.1 with fundamental parameters and by FULLPROF with a Pseudo-Voigt peak shape function are similar within experimental errors (Mitchell et al. 2004).

The ATOMS-6.0 software package (Dowty 1999) was used to determine interaxial angles describing the distortion of coordination polyhedra and selected bond lengths. The IVTON 2.0 program (Balić-Žunić and Vicković 1996) was employed to characterize the coordination spheres of the cations, volumes of coordination polyhedra, and displacements of cations from the centres of coordination polyhedra.

Results

Synthetic ordered titanates of Ni

The complex $Ni_{1/2}Mn_{1/2}TiO_3$, $Ni_{1/2}Mg_{1/2}TiO_3$, $Ni_{1/3}Zn_{1/3}Mg_{1/3}TiO_3$, and $Ni_{1/4}Zn_{14}Mg_{1/4}Mn_{1/4}TiO_3$ titanates isostructural with ilmenite were successfully and repeatedly prepared at 1095°C. Of the end member compounds, $MnTiO_3$ and $NiTiO_3$ were also prepared and used as reference materials. The $ZnTiO_3$ compound could not be prepared using our synthesis method.

Although the final products contained minor rutile, bunsenite-type solid solutions (cubic *A*O with varying amounts of Ni, Mg), spinel, and/or armalcolite-type titanates, the SEM QEDS analysis indicated that their compositions were of $ATiO_3$ stoichiometry within the limits of accuracy of the technique. The powder XRD patterns of all titanates considered here contain reflections *h0l* (*l* odd) (Fig. 2) which result from the ordered distribution of A^{2+} and Ti^{4+} in alternate layers of octahedra in the $R\bar{3}$ structure (Raymond and Wenk 1971), and are forbidden for the structures which adopt the $R\bar{3}c$ and $R3c$ space groups (Wechsler and Prewitt 1984; Ko and Prewitt 1988). Of note, these *h0l* (*l* odd) reflections become diffuse-to-absent in the XRD patterns of titanates of Ni subjected to further sintering in a non-buffered air atmosphere, thus suggesting considerable deviation from the $R\bar{3}$ structure due to a partial-to-complete disorder. Such partially disordered titanates formed in an open-air atmosphere are not considered further here.

Some Bragg reflections, arising from the presence of minor phases, are very close to or overlap with reflections of the major $R\bar{3}$ titanate phase (Fig. 2). Our experience shows that this overlap affects the accuracy of the determination of the amounts of the phases present by the Rietveld method (Liferovich and Mitchell 2004; Mitchell and Liferovich 2004). This overlap leads to slight overestimation of the abundance of armalcolite and bunsenite-like solid solutions as compared to that determined by SEM–BSE imaging (Note, the overall abundance of all minor phases in the titanates synthesized does not exceed 5 vol.%). The crystal structure parameters obtained using the approach described here for the impurity-bearing $MnTiO_3$ (pyrophanite) and $NiTiO_3$ samples, are almost identical to those obtained on single crystals of these titanates as determined by Kidoh et al. (1984) and Ohgaki et al. (1988), respectively. Thus, we are confident that the effects of reflection overlaps are not significant for this study.

Rietveld refinement and geometry of the sites

Voigt, pseudo-voigt and fundamental parameter approaches were tried for fitting the reflection profiles giving comparable *R*-values and statistically close positional parameters for refined sites. Finally, the fundamental parameter mode was used for refinements because it utilizes a convolution-based profile which reduces the number of definable profile parameters and thus eliminates many problems related to over-parameterization such as refinement of redundant parameters and parameter correlations (e.g. see p. 68 in Bruker 2003). Another advantage of the fundamental parameter approach to line profile fitting is that the fitted lattice parameters are automatically corrected for the line profile shifts arising from instrumental aberrations. Scattering factors of neutral atoms from International Tables for Crystallography were employed during the refinement. The size of crystallites was estimated using the "Sherrer equation" (Young 1995; Bruker 2003).

Depending upon the presence of impurities, the number of TOPAS 2.1 refined variables ranged up to 42 independent parameters. These included: zero corrections; scaling factors; cell dimensions; atomic positional coordinates; preferred orientation corrections; crystal size and strain effects; and isotropic thermal parameters. The background was modelled using a 6th-order Chebyshev polynomial. A fourth-order spherical harmonics series were employed for correction of preferred orientation effects. The occupancy of the ^{vi}A site was set in accordance with the target solid solution composition during initial steps and refined at the final steps of the procedure with the total occupation of the *Ti* and *A* sites constrained to unity.

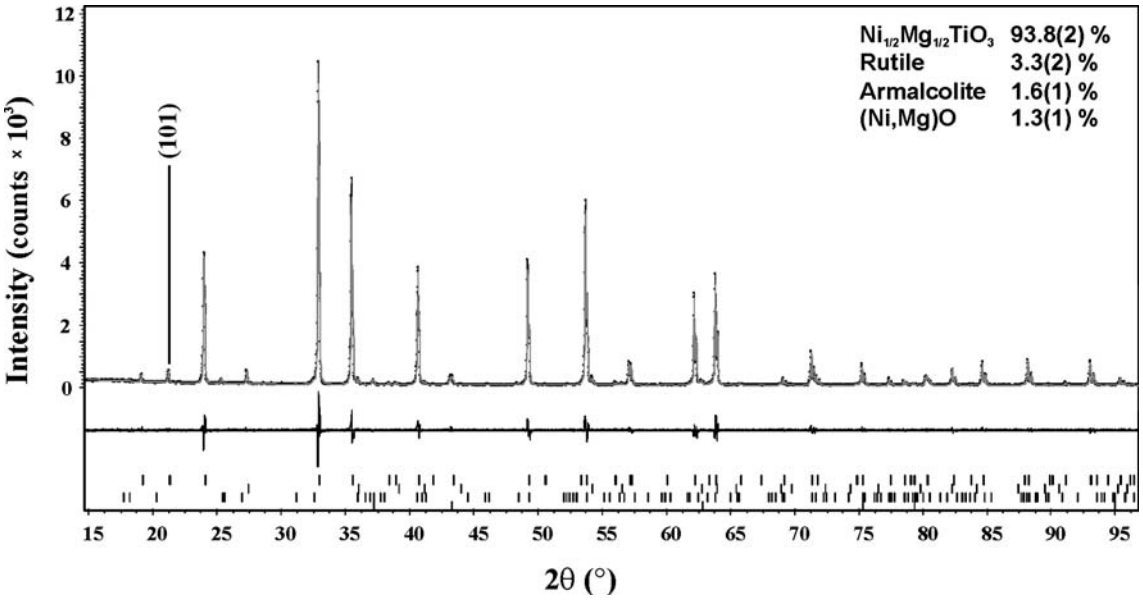

Fig. 2 A part of the Rietveld refinement plot (*line*) of the X-ray powder diffraction data for $Ni_{1/2}Mg_{1/2}TiO_3$ at room temperature (*dots*). The difference curves between observed and calculated profiles are plotted. For the agreement factors see Table 1. *Note*: The full X-ray diffraction pattern obtained for 2θ range from 10 to 120° was employed for the Rietveld refinement

For Rietveld refinement, we used the atomic coordinates given by Ohgaki et al. (1988) for synthetic $NiTiO_3$ as a starting model. Figure 2 is a portion of the Rietveld refinement plot for $Ni_{1/2}Mg_{1/2}TiO_3$. Given the small volume fractions of the minor contaminant oxide phases (Table 1), the atomic coordinates for these phases were fixed during the refinements. Restraints for bond lengths in the $ATiO_3$ titanates were not applied as refinements converged rapidly and easily. Positional parameters were refined stepwise from heavier to lighter cations with those of the oxygen anions last. Thermal parameters were refined as an isotropic approximation. Thermal parameters for cations sharing the *A*-site were constrained to be equal during refinements. With the above constraints incorporated into the Rietveld routine, refinement is rapid and the correlation between the occupancies, the scale parameters and the fractional coordinates is small. At a final step of the refinement procedure we attempted to refine occupancies of the ^{vi}A and ^{vi}Ti sites to test the possible entry of the divalent cation(s) into the ^{vi}Ti position and vice versa. These refinements converged easily (in a few steps) and did not induce statistically considerable changes in any of the refined parameters. The refined occupancies of both octahedral sites do not deviate from the target stoichiometry within the range of one estimated standard deviations (*e.s.d.*), i.e. neither the presence of Ti in the ^{vi}A site or/and any of divalent cations in the ^{vi}Ti site was indicated within the accuracy of the Rietveld method. This implies an absence of detectable disorder in the titanates of Ni considered here and agrees with the presence in their XRD patterns of the sharp *h0l* (*l* odd) reflections (Fig. 2) which are known to result from A^{2+}/Ti^{4+} ordering (Raymond and Wenk 1971). These should become diffuse-to-absent for disorder of the octahedrally coordinated cations.

Refined unit cell parameters and agreement factors, mean bond lengths within coordination octahedra, polyhedra volumes, displacements of $^{vi}A^{2+}$ and $^{vi}Ti^{4+}$ atoms from the centres of coordination polyhedra, bond lengths and bond angle distortion parameters are listed in Table 1, together with similar data calculated for synthetic $MnTiO_3$ and $NiTiO_3$ (this study). We tabulated these data in order of decreasing mean $^{vi}R_A^{2+}$ assuming that all divalent cations are in the high-spin state. The atomic positional parameters, deviation of observed z_A^{2+} and z_{Ti}^{4+} parameters from their ideal values (1/3 and 1/6, respectively), and isotropic displacement factors ($Å^2$) are listed in Table 2. Selected bond lengths and bond angles are given in Appendix 1.

To illustrate the polyhedron bond length distortion, we employ the Δ_n distortion index introduced by Shannon (1976) as $\Delta_n = \frac{1}{n} \cdot \Sigma\{(r_i - \bar{r})/\bar{r}\}^2 \cdot 10^3$, where $\bar{r}$ and r_i are average and individual bond lengths in the polyhedron, respectively. We describe deviations from the ideal bond angles appearing in a regular octahedron, by calculation of the bond angle variance index, $\delta_i = \Sigma\,[(\theta_i - 90)^2/(n-1)]$, where θ_i are the O–*A*–O or O–Ti–O bond angles (Robinson et al. 1971). The indices calculated, plus selected bond lengths and angles, are given in Table 1 and Appendix 1, respectively.

In common with ilmenite-structured $Mg_{1-x}Zn_xTiO_3$ and $Mn_{1-x}Zn_xTiO_3$ (Liferovich and Mitchell 2004; Mitchell and Liferovich 2004), occupation of the AO_6 site by mixtures of cations ranging in size from 0.83 to 0.69Å (Table 1), results in significant variations of the unit cell parameters and distortion indices of the coordination polyhedra. Unit cell dimensions and unit cell volumes of the Ni titanates decrease with decreasing average $^{vi}R_A^{2+}$ (Table 1). The average $<A–O>$ bond

Table 2 Positional parameters and isotropic displacement factors (Å^2) of synthetic titanates at ambient conditions

Position	Sample	x	y	Z	d_z	B_{iso}
^{vi}A	$MnTiO_3$	0	0	0.3602(1)	0.0269	0.25(3)
	$Ni_{1/2}Mn_{1/2}TiO_3$	0	0	0.3554(2)	0.0221	0.19(6)
	$Ni_{1/4}Mn_{1/4}Zn_{1/4}Mg_{1/4}TiO_3$	0	0	0.3578(2)	0.0244	0.56(5)
	$Ni_{1/3}Zn_{1/3}Mg_{1/3}TiO_3$	0	0	0.3555(2)	0.0221	0.57(6)
	$Ni_{1/2}Mg_{1/2}TiO_3$	0	0	0.3518(2)	0.0184	0.44(4)
	$NiTiO_3$	0	0	0.3506(1)	0.0173	0.34(6)
^{vi}Ti	$MnTiO_3$	0	0	0.1478(1)	−0.0189	0.30(3)
	$Ni_{1/2}Mn_{1/2}TiO_3$	0	0	0.1454(3)	−0.0213	0.12(5)
	$Ni_{1/4}Mn_{1/4}Zn_{1/4}Mg_{1/4}TiO_3$	0	0	0.1459(2)	−0.0208	0.22(4)
	$Ni_{1/3}Zn_{1/3}Mg_{1/3}TiO_3$	0	0	0.1452(2)	−0.0214	0.36(5)
	$Ni_{1/2}Mg_{1/2}TiO_3$	0	0	0.1448(1)	−0.0219	0.26(3)
	$NiTiO_3$	0	0	0.1445(1)	−0.0222	0.18(5)
O(1)	$MnTiO_3$	0.3200(6)	0.0292(8)	0.2426(4)		0.16(6)
	$Ni_{1/2}Mn_{1/2}TiO_3$	0.3169(6)	0.0247(10)	0.2445(4)		0.30(6)
	$Ni_{1/4}Mn_{1/4}Zn_{1/4}Mg_{1/4}TiO_3$	0.3202(6)	0.0240(10)	0.2462(5)		0.60(5)
	$Ni_{1/3}Zn_{1/3}Mg_{1/3}TiO_3$	0.3188(7)	0.0197(10)	0.2442(4)		0.20(5)
	$Ni_{1/2}Mg_{1/2}TiO_3$	0.3183(5)	0.0192(8)	0.2460(2)		0.33(5)
	$NiTiO_3$	0.3151(7)	0.0178(10)	0.2455(3)		

d_z deviation from ideal value of the z positional parameter (1/3 and 1/6 for ^{vi}A and ^{vi}Ti atoms, respectively, *see* Fig. 1b for details)

length becomes less with decrease in the size of the $^{vi}A^{2+}$ cation. The average $<$Ti-O$>$ bond length in all the titanates is not affected by cationic substitutions at the A site within the accuracy of determination (Table 1), and is identical to those obtained by high-precision methods on single crystals of $MnTiO_3$ (Kidoh et al. 1984) and $NiTiO_3$ (Ohgaki et al. 1988) (1.980[1] and 1.983[1]Å, respectively). The absence of compositionally driven changes in the $<$Ti–O$>$ bond length of the diverse $ATiO_3$ titanates prepared here indicates that the considerably larger Mn^{2+}, Mg^{2+}, Zn^{2+}, and Ni^{2+} cations do not replace the smaller $^{vi}Ti^{4+}$ cation, as this should result in enlargement of the (Ti,A)O$_6$ octahedra and increase of the average $<$(Ti,A)–O$>$ bond length.

All the titanates consist of distorted coordination polyhedra, similar to those occurring in pyrophanite, geikielite, $NiTiO_3$, and ilmenite sensu lato. The TiO_6 octahedra have relatively high bond length and bond angle distortion parameters and are distorted to nearly the same extent in all the titanates investigated (Table 1). The AO_6 octahedra exhibit less but more variable bond length distortion in comparison to those of the TiO_6 octahedra. Bond angle distortion indices calculated for the AO_6 octahedra are greater for large A-cation titanates and decrease nearly regularly with decreasing $^{vi}R_A^{2+}$ (Table 1).

In the titanates with the larger average A-site cations, the A atoms have a greater displacement from centres of the coordination polyhedra than the Ti atoms, and vice versa in the titanates of the lesser average A^{2+} (Table 1). This observation is in accord with the deviation of the z positional parameter from its theoretical value (listed as d_z in Table 2), i.e. shift of the atom along the threefold axes, which results in "puckering" (Wechsler and Prewitt 1984) of the octahedral layers above and below planes parallel to (001) as illustrated in Fig. 1b. Comparison of these deviations shows that in the titanates with $^{vi}R_A^{2+} \geq 0.71$Å and $t \geq 0.745$ (mean A^{2+} cation size and Goldschmidt tolerance factor, respectively), the layers of the AO_6 octahedra are more "puckered" above and below planes parallel to (001) as compared to the layers of the TiO_6octahedra and vice versa in the titanates with the smaller A^{2+} cations, in which $^{vi}R_A^{2+} \leq 0.71$Å and $t \leq 0.745$ (Tables 1, 2).

Distortion of coordination polyhedra in the nickel titanates studied here might result from possible complex interactions of $^{vi}Ni^{2+}$ which has a d^8 configuration in the high-spin state and can exhibit a first order Jahn–Teller effect (Orgel 1960), and interference of this distortion with that arising from an electronic second-order Jahn–Teller effect occurring around the $^{vi}Ti^{4+}$ cations (Kunz and Brown 1995). "Direct $^{vi}A^{2+}$–$^{vi}A^{2+}$ interactions within (111) planes" are possible for Ni, Co, and Mn and in some cases may be even stronger than the $^{vi}A^{2+}$–O–O–$^{vi}A^{2+}$ interactions (Goodenough 1960). The repulsive Ti–Ti and A–Ti interactions across the shared faces and edges of octahedra are well-known and induce displacement of cations from their otherwise regular positions, resulting in distortion of the coordination polyhedra in the $R\bar{3}$-structured titanates (Wechsler and Prewitt 1984; Ko and Prewitt 1988; Harrison et al. 2000). According to Ohgaki et al. (1988), a considerable metal–metal bonding occurs in $NiTiO_3$ along the threefold axis between neighbouring Ni^{2+} and Ti^{4+} cations, although anharmonicity of the thermal parameters for the cations at room temperature is small. Neither of these complex interactions, if any, result in detectable reduction of the mean bond length of the TiO_6 octahedra and/or A:Ti disorder in any nickeliferous titanates.

Conclusion

The $Ni_{1/2}Mn_{1/2}TiO_3$, $Ni_{1/2}Mg_{1/2}TiO_3$, $Ni_{1/3}Zn_{1/3}Mg_{1/3}TiO_3$, and $Ni_{1/4}Zn_{14}Mg_{1/4}Mn_{1/4}TiO_3$ titanates adopt

ordered rhombohedral ilmenite-like structures and are stable at ambient conditions. A completely ordered distribution of the A^{2+} and Ti^{4+} cations in all the non-oxidized stoichiometric rhombohedral titanates considered here is in agreement with data of Ko and Prewitt (1988) who demonstrated the absence of *A*:Ti disorder in the synthetic ternary titanates up to the melting point using a single-crystal of $MnTiO_3$ as an example.

The decrease in the lattice ratios, c/a (Table 1), which is equal to $\sqrt{8}$ ~2.828 for an ideal hexagonal close packing, indicate increasing departure from ideal *hcp* and the *archetype* corundum structure induced by decrease in the size of the $^{vi}A^{2+}$ cations. The compositionally driven style of deformation observed for the $R\bar{3}$-structured titanates studied here results in the decrease of $d_z(A)$ along with increase in d_z(Ti). This style of deformation is opposite to that described for the *aristotype* ilmenite at high pressure or high temperature (Wechsler and Prewitt 1984), both of which induce increase of $d_z(A)$ and decrease of d_z(Ti).

Our data imply the existence of binary, ternary, and quaternary solid solutions between $NiTiO_3$ and $MnTiO_3$ (pyrophanite), $MgTiO_3$(geikielite), and $ZnTiO_3$ (ecandrewsite) and demonstrates the tolerance of the ordered $R\bar{3}$ structure to wide variations in the average radius of the divalent cation in the ^{vi}A position, resulting in Goldschmidt tolerance factors, *t*, ranging from 0.786 to 0.737. The scarcity of natural ilmenite-group minerals containing significant amounts of Ni is not due to crystallochemical limitations, but arises from the differing geochemistry of Ni relative to that of Ti, Mn, Mg, or Zn in natural systems. Formation of the nickeliferous ilmenite-structured solid solutions might be possible in some exotic mineral-forming or metamorphic environments at low pressures and/or in extraterrestrial rocks.

Acknowledgements This work is supported by the Natural Sciences and Engineering Research Council of Canada and Lakehead University (Canada). We thank Allan MacKenzie for assistance with analytical work, and Anne Hammond for sample preparation. The authors are grateful to Dr. K. Garbev and an anonymous reviewer whose constructive criticism resulted in improvements to

			1	*2*	*3*	*4*	*5*	*6*
AO_6 octahedron								
3×*A*-O1		Å	2.100(4)	2.085(5)	2.046(5)	2.045(5)	2.052(3)	2.059(4)
3×*A*-O1		Å	2.292(5)	2.197(6)	2.212(6)	2.197(5)	2.139(3)	2.117(4)
3×O–*A*–O		°	73.01	75.45	75.78	76.13	78.25	78.25
3×O–*A*–O		°	91.61	91.08	90.12	90.75	90.34	90.35
3×O–*A*–O		°	88.45	89.12	87.83	89.47	89.21	89.94
3×O–*A*–O		°	103.06	101.44	102.96	100.99	100.11	99.50
3×O–*A*–O		°	158.57	161.54	160.48	162.38	164.16	164.97
TiO_6 octahedron								
3×Ti-O1		Å	1.876(4)	1.862(5)	1.863(5)	1.850(5)	1.856(3)	1.858(4)
3×Ti-O1		Å	2.086(5)	2.084(5)	2.103(6)	2.082(5)	2.096(3)	2.079(4)
3×O–Ti–O		°	162.59	161.37	162.53	162.23	162.07	161.47
3×O–Ti–O		°	81.04	80.37	80.47	81.19	80.16	79.98
3×O–Ti–O		°	81.63	81.32	82.40	81.70	82.59	82.24
3×O–Ti–O		°	94.12	93.20	93.34	91.47	92.13	91.84
3×O–Ti–O		°	101.92	103.16	102.08	103.54	102.98	103.59
A–Ti		Å	3.035	2.945	2.960	2.917	2.867	2.843
A-*A*	*a*	Å	3.065	3.001	3.010	2.982	2.955	2.944
A-*A*	*b*	Å	3.993	4.053	3.975	4.010	4.106	4.120
Ti–Ti	*a*	Å	3.015	2.996	2.988	2.978	2.973	2.969
Ti–Ti	*b*	Å	4.223	4.076	4.077	4.030	4.010	3.985
O–O	*c*	Å	2.728	2.689	2.717	2.709	2.699	2.672
O–O	*d*	Å	3.287	3.228	3.201	3.156	3.146	3.143
O–O	*e*	Å	3.152	3.058	3.016	3.021	2.973	2.962
O–O	*f*	Å	3.066	3.006	2.955	2.988	2.944	2.952
O–O	*g*	Å	2.915	2.917	2.897	2.907	2.904	2.920
O–O	*h*	Å	2.580	2.576	2.619	2.578	2.614	2.594
O–O	*i*	Å	2.904	2.870	2.890	2.820	2.851	2.832
Ti–O–*A*	*j*	°	119.31	119.25	120.05	120.37	120.62	120.00
A–O–*A*	*k*	°	88.38	89.92	89.88	89.25	89.66	89.65
Ti–O–Ti	*l*	°	98.96	98.67	97.60	98.30	97.41	97.76
Ti–O–*A*	*m*	°	126.21	127.87	126.94	128.50	129.05	129.80
Ti–O–*A*	*n*	°	87.61	86.88	86.60	85.90	85.20	85.31
Ti–O–*A*	*o*	°	136.64	135.56	135.64	134.08	134.48	134.19

1 $MnTiO_3$; *2* $Ni_{1/2}Mn_{1/2}TiO_3$; *3* $Ni_{1/4}Mn_{1/4}Zn_{1/4}Mg_{1/4}TiO_3$; *4* $Ni_{1/3}Zn_{1/3}Mg_{1/3}TiO_3$; *5* $Ni_{1/2}Mg_{1/2}TiO_3$; *6* $NiTiO_3$

The metal–metal distances: *a* across shared edge between adjacent metal sites; *b* across vacant octahedral position

The oxygen–oxygen distances: *c* *A*-Ti shared face; *d* *A* site, face opposite the shared face; *e* *A* site, shared edge; *f* *A* site, unshared edge; *g* Ti site, face opposite the shared face; *h* Ti site, shared edge; *i* Ti site, unshared edge

Framework angles: *j*, *m*, and *o* at the shared vertex; *k* and *l* at the shared edge; *n* shared face

the initial version of this work. The authors also would like to thank Dr. Catherine McCammon for editorial care in handling of this contribution.

Appendix 1

Selected bond lengths (Å) and bond angles (°) of synthetic titanates at ambient conditions

References

Badjukov DD, Raitala J, Petrova TL (2001) Ni–Co, Cu, and Zn sulphides in the melt rocks of the Saaksjarvi crater: characteristics and their possible origin. In: 32nd Ann Lunar Planet Science Conf Houston, Texas, http://www.lpi.usra.edu/meetings/lpsc2001/pdf/1532.pdf

Balić-Žunić T, Vicković I (1996) IVTON—a program for the calculation of geometrical aspects of crystal structures and some crystal chemical applications. J Appl Crystallogr 29:305–306

Boysen H, Frey F, Lerch M, Vogt T (1995) A neutron powder investigation of the high-temperature phase transition in $NiTiO_3$. Zeitschr Krystallogr 210:328–337

Bruker AXS (2001) Powder diffraction file (PDF). Release 2001, Bruker AXS GmbH

Bruker AXS (2003) TOPAS 2.1: General profile and structure analysis software for powder diffraction data. User's Manual, Bruker AXS. Karlsruhe, Germany, p 79

Cheary RW, Coelho AA (1992) A fundamental parameters approach to X-ray line profile fitting. J Appl Crystallogr 25:109–121

Coelho AA (2000) Whole-profile structure solution from powder diffraction data using simulated annealing. J Appl Crystallogr 33:899–908

Dowty E (1999) *Atoms 5.0*. By Shape Software, Kingsport, TN 37663, USA, http://shapesoftware.com/

Goldschmidt VM (1926) Naturwissenschaft 14:477–485 (not seen; a cross-reference from Lufaso MW, Woodward PM [2001] Prediction of the crystal structures of perovskites using the software program SPuDS. Acta Cryst B57:725–738)

Goodenough JB (1960) Direct cation–cation interactions in several oxides. Phys Rev 117:1442–1451

Harrison RJ, Becker U, Redfern AT (2000) Thermodynamics of the $R\bar{3}$ to $R\bar{3}c$ phase transition in the ilmenite-hematite solid solution. Am Mineral 85:1694–1705

Kidoh K, Tanaka K, Marumo F, Takei H (1984) Electron density distribution in ilmenite-type crystals. II. Manganese (II) titanium (IV) trioxide. Acta Crystallogr B40:329–332

Ko J, Prewitt C (1988) High-pressure phase transformation in $MnTiO_3$ from the ilmenite to the $LiNbO_3$ structure. Phys Chem Mineral 15:355–362

Kunz M, Brown ID (1995) Out-of-center distortions around octahedrally coordinated d^0-transition metals. J Solid State Chem 115:395–406

Lerch M, Laqua W (1992) Zur thermodynamic und elektrischen Leitfähigkeit von $NiTiO_3$und anderen oxidischen Phasen mit Ilmenit-structur. Z Anorg Allg Chem 610:57–63

Lerch M, Stüber C, Laqua W (1991) Aspekte eines Hochtemperatürgangs in $NiTiO_3$. Z Anorg Allg Chem 594:167–179

Lerch M, Boysen H, Neder R, Frey F, Laqua W (1992) Neutron scattering investigation of the high temperature phase transition in $NiTiO_3$. J Phys Chem Solids 53:1153–1156

Liferovich RP, Mitchell RH (2004) Geikielite-ecandrewsite solid solutions: synthesis and crystal structures of the $Mg_{1-x}Zn_xTiO_3$ ($0 \leq x \leq 0.8$) series. Acta Crystallogr B60:496–501

Linton JA, Fei Y, Navrotsky A (1999) The $MgTiO_3$-$FeTiO_3$ join at high pressure and temperature. Am Mineral 84:1595–1603

Mitchell RH (2002) Perovskites: Modern and Ancient. Almaz Press, Thunder Bay, pp 318 (http://www.almazpress.com)

Mitchell RH, Liferovich RP (2004) Pyrophanite–ecandrewsite solid solution, part II: synthetic $Mn_{1-x}Zn_xTiO_3$ ($0.1 \leq x \leq 0.8$) series and its crystal structure characteristics. Can Mineral 42:1871–1880

Mitchell RH, Ross KC, Potter EG (2004) Crystal structures of $CsFe_2S_3$ and $RbFe_2S_3$: synthetic analogs of rasvumite KFe_2S_3. J Solid State Chem 177:1867–1872

Ohgaki M, Tanaka K, Marumoto F, Takei H (1988) Electron density distribution in ilmenite-type crystals III. Nickel (II) titanium (IV) trioxide, $NiTiO_3$. Mineral J (Japan) 14:133–144

Orgel LE (1960) An introduction to the transition-metal chemistry ligand-field theory. Methuen, London, p 180

Raymond KN, Wenk HR (1971) Lunar ilmenite (Refinement of the crystal structure). Contrib Mineral Petrol 30:135–140

Rietveld HM (1969) A profile refinement method for nuclear and magnetic structures. J Appl Crystallogr 2:65–71

Robinson K, Gibbs GV, Ribbe PH (1971) Quadratic elongation: a quantitative measure of distortion in coordination polyhedra. Science 172:567–570

Rodriguez-Carvajal JJ (1990) ''FULLPROF'' program: Rietveld pattern matching analysis of powder patterns. ILL, Grenoble

Shannon RD (1976) Revised effective ionic radii and systematic studies of interatomic distances in halides and chalcogenides. Acta Crystallogr A32:751–767

Syono Y, Akimoto S, Ishikawa Y, Endoh Y (1969) A new high pressure phase of $MnTiO_3$ and its magnetic property. J Phys Chem Solids 30:1665–1672

Wechsler BA, Prewitt C (1984) Crystal structure of ilmenite ($FeTiO_3$) at high temperature and high pressure. Am Mineral 69:176–185

Young RA (ed) (1995) The Rietveld method. Oxford University Press Inc, New York, p 298